DTU Compute

Department of Applied Mathematics and Computer Science

Dynamics of adaptive neuronal networks
A trip to topology and back

Author
Simon Aertssen
s181603

Supervisor
Erik Martens
Poul Hjorth

February 1$^{\text{st}}$ 2020

Contents

Abstract

Lorem ipsum dolor sit amet, consectetur adipiscing elit. Quisque nisl eros, pulvinar facilisis justo mollis, auctor consequat urna. Morbi a bibendum metus. Donec scelerisque sollicitudin enim eu venenatis. Duis tincidunt laoreet ex, in pretium orci vestibulum eget.

Acknowledgements

1 Nomenclature

i, e (or $\exp$)	Imaginary unit. Euler's number.
$n, \deg(n)$	Network node. Degree of node n.
N	Network degree. The number of neurons in the network.
A_{ij}	Adjacency matrix. Models which neuron i is connected to neuron j and vice-versa.
$\langle k \rangle$	Average node degree in the network.
$\boldsymbol{k}$	Node degree. Vector of the in- and out-degree of a single node as $\left(k^{\text{in}}, k^{\text{out}}\right)$.
$\boldsymbol{k^{\text{in}}}, \boldsymbol{k^{\text{out}}}$	Node degree vector of all in- and out degrees of the network.
$M_{\boldsymbol{k}}$	Number of unique node degrees in the network.
$P(k), P(\boldsymbol{k})$	Univariate and bivariate network degree distribution.
$k_{\text{min}}, k_{\text{max}}$	Smallest and largest degree found in a network.
γ	Degree exponent of a scale-free network.
p	Probability threshold of forming a link in random networks.
c	Assortativity of the network.
$\theta(t)_i$	Phase variable function of the theta model (of neuron i).
$\mathcal{P}_n(\theta)$	Pulse shaped synaptic coupling function.
κ	Macroscopic coupling strength.
$\eta_i, I(t)_i$	Excitability threshold and input current (of neuron i).
$g(\eta|\eta_0, \sigma)$	Excitability threshold distribution with mean η_0 and width σ.
$Z(t)$	Kuramoto order parameter function.
$z(\boldsymbol{k}, t)$	Order parameter function for nodes with degree $\boldsymbol{k}$.
$\bar{Z}(t)$	Mean field order parameter function for arbitrary networks.
$S^{\text{in}}(t)_i, S^{\text{out}}(t)_i$	Spike trains received and emitted by neuron i as a sum of delta functions in time.
K_{ij}	Synaptic connectivity matrix. Strength of the connections between neurons i and j.
Δt_{ij}	Time difference between spikes of neurons i and j.
$W(\Delta t_{ij})$	Learning window. Models the correlation between synaptic strength and spike times.
$\phi(\Delta t_{ij})$	IP learning function. Models correlation between excitability strength and spike times.
$\mathbb{T}$	Set of angles in $[-\pi, \pi[$.
$\mathbb{K}$	Set of unique degrees in a network, support of P.
$\mathbb{R}, \mathbb{C}$	Set of real numbers. Set of complex numbers.
$\mathcal{F}(v), \mathcal{F}^{-1}(v)$	Random permutation and inverse permutation of the elements of a vector v.

2 Introduction

In 2013, one of the largest scientific projects ever funded by the European Union was launched. With the Human Brain Project [1], scientists and researchers aimed to reconstruct the human brain through supercomputer-based models and to advance neuroscience, medicine, and computing. Across the globe different fields of science are drawing inspiration from the human brain, through different approaches.

One such approach is to model the behaviour of biological neurons and to quantify the information processes in the brain from stimuli from the senses or from electrical and chemical processes in the body. A given neuron receives hundreds of impulses in the form of neurotransmitters, almost exclusively on its dendrites and cell body. These stimuli add up to an excitatory or inhibitory influence on the membrane potential of the neuron, so that the potential spikes when excitation is higher than an internal threshold. At this point, the neuron releases its own neurotransmitter and joins the interneuronal communication [2]. The neuron dynamics are largely captured by this spiking behaviour, on which most efforts have been concentrated. In 1952, Hodgkin and Huxley described a mathematical model for the action potentials in neurons, using a set of nonlinear differential equations that approximates the electrical characteristics of the neuron elements. In 1963 the authors were awarded the Nobel Prize in Physiology or Medicine [3] for their work.

As the human brain contains more than 100 billion neurons [4] it is unfeasible to study complex models at this scale. The topology of neuronal networks displays traits of small-worldness, wiring optimisation, and heterogeneous degree distributions [5], for which it is difficult to pin down one type of network architecture. Through the mean-field reduction (*MFR*) proposed in [6] one can reduce a large network of indistinguishable neurons to a low-dimensional dynamical system, described by the attraction of a mean-field variable to a reduced manifold. In this paper we will study the *MFR* of different types of networks of coupled theta neurons using the generalisations found in [7].

3   Network Topologies

Networks consists of *nodes* n_j, $j \leq N$ connected by *links*. They arise in any context where objects are *related* to each other.

3.1   Representations and properties

We represent a finite network through the adjacency matrix: $A_{ij} = 1$ if there exists a relation from node j to node i and 0 otherwise. This means that A_{ij} can be *undirected* (symmetric) or *undirected*. If we think of the relations between guests at a party, then the social network is directed, as people might not know each other mutually. However, the network of people having shaken hands is symmetric. Self-links are an edge-case that depends on the context, as one generally does not shake hands with himself.

From A_{ij} we can compute the in- and out-degree vectors, which show how many links a node has coming in and out:

$$\boldsymbol{k}_i^{\text{in}} = \sum_{j=1}^{N} A_{ij} \qquad \boldsymbol{k}_j^{\text{out}} = \sum_{i=1}^{N} A_{ij} \qquad \deg(n_j) = \boldsymbol{k}_j = (\boldsymbol{k}_j^{\text{in}}, \boldsymbol{k}_j^{\text{out}}) \in \mathbb{K} \subset \mathbb{N} \qquad (1)$$

The distribution of $\boldsymbol{k}^{\text{in}}$ and $\boldsymbol{k}^{\text{out}}$ is the most defining property of the network:

$$(\boldsymbol{k}^{\text{in}}, \boldsymbol{k}^{\text{out}}) \sim P(\deg(n) = \boldsymbol{k}) \qquad (2)$$

The support of P is the set of unique degrees $\mathbb{K}$ with cardinality $M_{\boldsymbol{k}}$, which consists of integers. For symmetric networks, $\boldsymbol{k}^{\text{in}} = \boldsymbol{k}^{\text{out}}$, so that P is really a univariate distribution.

3.2   Fixed-degree networks

A network consists of nodes, connected by links. The most simple network is one where all the nodes are connected, and so all nodes have a degree of N. In general, we can make networks where all nodes have the same degree, $\langle k \rangle$:

$$P(k) = \begin{cases} \langle k \rangle & \text{if } k = \langle k \rangle \\ 0 & \text{otherwise} \end{cases} \qquad \mathbb{K} = \{\langle k \rangle\} \qquad (3)$$

We will refer to these networks as fixed-degree networks.

3.3   Random / Erdös-Rény networks

In 1959 Erdös and Rény published their work on random graphs [8], where links are established if a random uniformly distributed number is higher than a threshold p. The degrees follow a binomial distribution:

$$P(k) = \binom{N-1}{k} p^k (1-p)^{N-1-k} \qquad \mathbb{K} = [0, N] \qquad (4)$$

with a mean $\mu = p(N-1)$ and standard deviation $\sigma = \mu(1-p)$. For networks where $\langle k \rangle \ll N$, the network can be well approximated by a Poisson distribution:

$$P(k) = e^{-\langle k \rangle} \frac{\langle k \rangle^k}{k!} \qquad \mathbb{K} = [0, N] \qquad (5)$$

with a mean $\mu = \langle k \rangle$ and standard deviation $\sigma = \sqrt{\langle k \rangle}$. Both (4) and (5) describe similar quantities, but the latter is used more often due to its analytical simplicity [9].

3.4 Scale-free networks

What we can often observe in nature is the preferential attachment to nodes with a high degree [5]: the rich or famous tend to get more rich or famous. This trait is also described as the 80/20 rule by Pareto. Networks with this property consist of a small number of highly connected nodes, and a large number of low degree nodes. We can represent this with a power law distribution:

$$P(k) = Ak^{-\gamma} \qquad \mathbb{K} = [k_{\min}, k_{\max}] \qquad (6)$$

with A is a constant so that $\sum_{k=1}^{\infty} P(k) = 1$. We can also see that $A \sum_{k=1}^{\infty} k^{-\gamma} = 1$ so that $A = \sum_{k=1}^{\infty} k^{\gamma} = 1/\zeta(k)$, the Riemann Zéta function [9].

Networks with a distribution like (6) are called *scale-free* networks, as they lack an internal scale to represent the magnitude of the network: we can observe (6) on different scales like the probability of two Hollywood actors appearing in a movie, or the connections between web pages on the internet [10]. One description that comes close is the *natural cutoff* $k_{\max}$, the expected degree of the largest degree in the network. As we only expect the largest hub to be the only hub in the domain $[k_{\max}, +\infty]$:

$$\int_{k_{\max}}^{\infty} P(k) dk = \frac{1}{N}$$

For (6) this results in:

$$k_{\max} = k_{\min} \cdot N^{\frac{1}{\gamma-1}} \qquad (7)$$

which shows that there might be large differences in size between the nodes.

There are constraints on γ to yield a scale-free network. When $0 < \gamma < 2$ the largest hub grows faster than N, so once its degree exceeds $N-1$ there are no more new nodes to connect to and the network will not be able to grow according to (6). A rigorous proof is given in [11]. For $\gamma = 2$, the system grows linearly, as we can see in (7). When $2 < \gamma \leq 3$ we find the most scale-free networks, as for $\gamma > 3$ hubs are not sufficiently large and numerous to have much influence on the network [9].
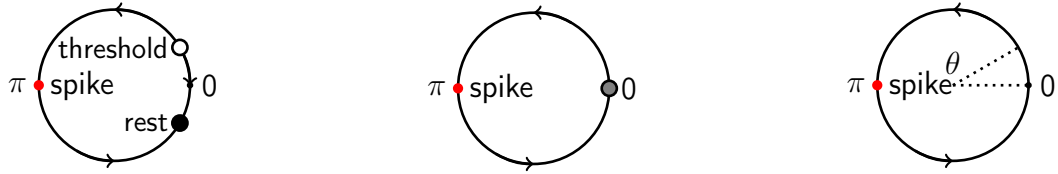
4 The Theta Neuron Model

A number of neuron model families have been identified, and often there exists a continuous change of variables from models of the same family into a *canonical* model that can represent the whole family [12]. As the transformation is not required to be invertible, we can study the universal neurocomputational properties of the family in a low dimensional model. It was Hodgkin [13] who classified neurons into two types based on their excitability, upon experimenting with the electrical stimulation of cells. Class 1 models begin to spike at an arbitrarily slow rate, and the spiking frequency increases when the applied current is increased. Class 2 models spike as soon as their internal threshold is exceeded and the spiking frequency stays relatively constant within a certain frequency band [12].

4.1 Model description

In [14], a class 1 canonical phase model was proposed:

$$\dot{\theta} = (1 - \cos\theta) + (1 + \cos\theta) \cdot I \qquad \theta \in \mathbb{T} \tag{8}$$

with I a bifurcation parameter on the supplied current. We can visualise the dynamics on the unit circle, like in Figure 1. The neuron produces a spike when θ surpasses π, upon which $\theta \leftarrow -\pi$.

Excitable regime: $I < 0$ Bifurcation: $I = 0$ Periodic regime: $I > 0$

Figure 1: SNIC bifurcation of the theta neuron model. A spike occurs when $\theta = \pi$. For $I < 0$, the neuron is in a rest state but *excitable*. For $I > 0$, $\dot{\theta} > 0$ so that θ moves continuously around the circle and we can observe *periodic* sustained spiking. The saddle-node bifurcation occurs at $I = 0$, so that θ will spike when it is larger than 0.

We can recognise the features of the class 1 model in Figure 2. This makes (8) the normal form of the *saddle-node-on-invariant-circle* (*SNIC*) bifurcation [15].
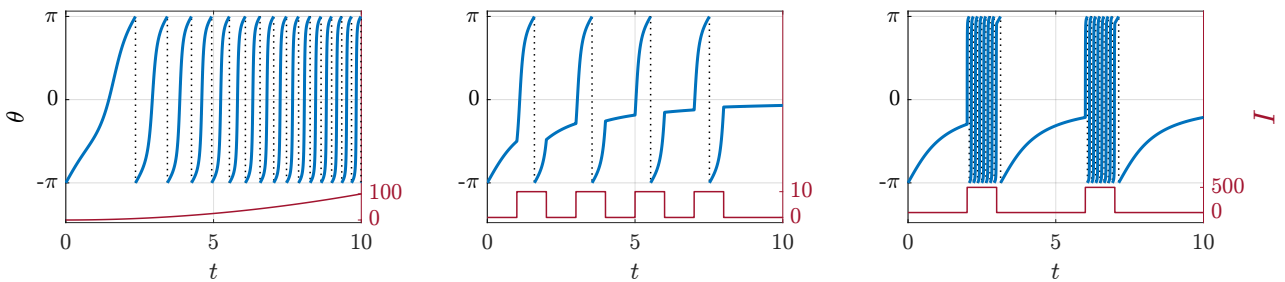

Figure 2: Properties of the theta neuron model, with solutions of (8) in blue, spikes marked in dotted lines, and the current I in red. Left: the spike frequency of θ increases as I is increased over time, which is the distinguishing feature of class 1 canonical models. Middle: spikes occur within a finite time period when $I > 0$ and within infite time when $I = 0$. Right: when I is large, the neuron *bursts*.

Equilibria only exist for the *excitable* regime $I < 0$:

$$\dot{\theta} = 1 - \cos\theta + I + I \cdot \cos\theta = (I + 1) + (I - 1) \cdot \cos\theta$$

$$\theta_{1,2}^* = \pm\arccos\left(\frac{I+1}{1-I}\right) + 2\pi n$$

We can find the stability of the equilibria through:

$$\frac{d}{d\theta}((1-\cos\theta)+(1+\cos\theta)\cdot I)=\sin\theta-\sin\theta\cdot I=(1-I)\cdot\sin\theta$$

In the equilibria this yields:

$$\frac{d}{d\theta}\left(\theta_{1,2}^*\right)=\pm(1-I)\cdot\sqrt{1-\frac{I+1}{1-I}}=\pm(1-I)\cdot\frac{2\sqrt{-I}}{1-I}=\pm2\sqrt{-I}$$

This yields a stable equilibrium point for θ_1^* and an unstable for θ_2^*. This means that as θ gets perturbed above θ_2^*, a spike occurs and θ converges to θ_1^*. This is demonstrated in Figure 3.
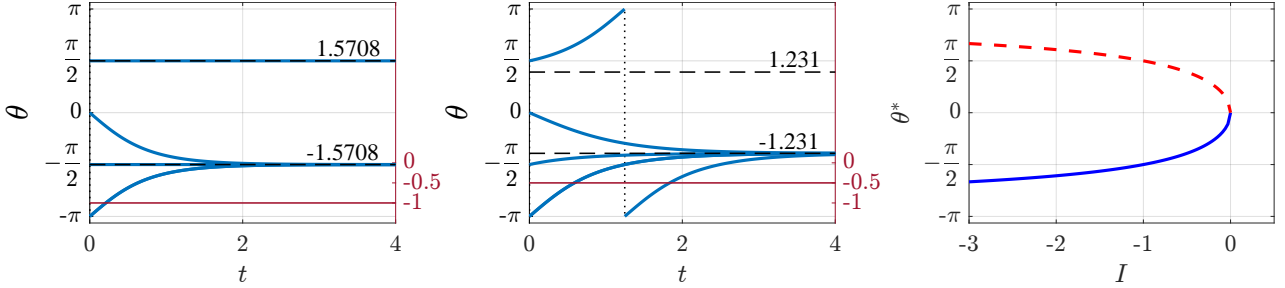

Figure 3: Equilibria θ^* for different values of I. Left: $I=-1$ yields $\theta_{1,2}^*=\pm\frac{\pi}{2}$, one of the simulations is started exactly on the unstable equilibrium. Middle: $I=-0.5$. Right: bifurcation diagram of the *SNIC* bifurcation, with the stable equilibria in blue, and the unstable in red.

4.2 Solutions for static currents

Gaining insight into (8) is hard, due to the difficulty of finding an analytical solution. However, it has been noted that there exists a simple transformation which yields (see A.1):

$$V\equiv\tan\left(\frac{\theta}{2}\right) \tag{9}$$

$$\dot{V}=V^2+I \tag{10}$$

This model is called the *Quadratic Integrate and Fire model* (*QIF*). (10) models the membrane potential of a neuron, which spikes to $=\infty$ when the neuron spikes and is reset at $-\infty$. The transformation (9) is continuous between spikes, so insights from a solution for V can be transformed directly. The equilibria of the *QIF* model are simply $\pm\sqrt{I}$ so that we can express $\theta_{1,2}^*=2\cdot\arctan\left(\mp\sqrt{I}\right)$, from [16].

The solution for the excitable regime $I<0$ is :

$$V(t)=\frac{2\sqrt{-I}}{1-e^{2t\sqrt{-I}}}-\sqrt{-I} \tag{11}$$

The solution at the bifurcation $I=0$ is :

$$V(t)=\frac{-1}{t} \tag{12}$$

The solution for the periodic regime $I>0$ is :

$$V(t)=-\sqrt{I}\cdot\cot(t\sqrt{I}) \tag{13}$$

These equations assume that at $t=0$ a spike has occured. he steps required to find (11)-(13) are described in A.2. Solutions for θ are found by taking the inverse of the transformation (9).

4.3 Frequency response

As we already saw in Figure 2, an increasing current increases the spiking frequency. We can compute this relationship by measuring how long it takes for V to reach a spike: we solve (13) for t at $V(t) = +\infty$ in A.3. This yields the oscillation period $T = \frac{\pi}{\sqrt{I}}$ which we can see in Figure 4. We know that when $\theta > \theta_2^*$ a spike occurs in the excitable regime, or in any case in the periodic regime. But the time that it takes to reach the spike can be arbitrarily long, depending on how far we are over θ_2^*. So, spikes will occur, but after a delay that is dependant on the stimulus. Explicitly, if we perturb $\theta(0) = \theta_2^* + \varepsilon$ we obtain from [16]:

$$T_{\text{spike}} = \frac{-\tanh^{-1}\left(1 + \frac{\epsilon}{\sqrt{I}}\right)}{\sqrt{I}}$$

The delay to the spike blows up as $\varepsilon \to 0$ so that spikes may occur after a very large delay.
In most of our future work, I will not be a static current. We ask ourselves: how sensitively does T depend on I when I is perturbed? We can measure this as a *relative* perturbation using dI/I and dT/T [2] :

$$\left|\frac{dT}{dI}\frac{I}{T}\right| = \left|\frac{dT/T}{dI/I}\right| = \left|-\frac{\pi}{2}\left(\frac{1}{\sqrt{I}}\right)^3\frac{I}{T}\right| = \left|\frac{\pi}{2}\left(\frac{T}{\pi}\right)^3\frac{I}{T}\right| = \frac{1}{2}\left|\left(\frac{T}{\pi}\right)^2\cdot\left(\frac{\pi}{T}\right)^2\right| = \frac{1}{2}$$

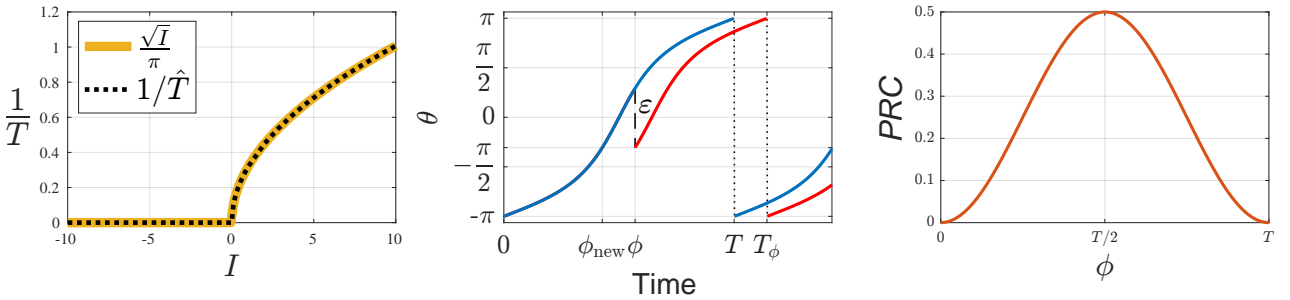Hence, a 1% change in I will result in a 0.5 % change in the period.

Figure 4: Response of the theta model to bifurcations on the frequency and the phase. Left: Frequency response of the theta model. For $I \leq 0$ the spike period is infinite, which is why we see the solutions to (8) approach $\theta = 0$ for $I = 0$. Middle: a bifurcation ε at time ϕ perturbs $\theta(t)$ (in blue) which results in a delayed spike (trajectory in red). Right: The *PRC*, (15) in red.

4.4 Phase response

Perturbations on the period can also be understood from the perspective of the phase. Changes to the phase θ can delay or advance the event of a spike, and in general this depends on exactly when the stimulus occurs. The phase response curve (*PRC*) gives us exactly that relation [16, 17]. Let us define $\phi \in [0, T[$, which represents the time since the last event of a spike. When we add a small bifurcation $\varepsilon < 0$ to θ at time ϕ, a spike will occur at T_ϕ, and we have that $\theta(\phi_{\text{new}}) = \theta(\phi) + \varepsilon$. The time to the new spike is $T_\phi = T + (\phi - \phi_{\text{new}})$. The *PRC* can then be defined as:

$$PRC(\phi) = T_\phi - T \tag{14}$$

This process has been visualised in Figure 4, after [17]. For infinitesimally small perturbations to the phase, we can find the *PRC* as the *adjoint* of the solution, [16], as:

$$PRC(\phi) = \frac{1}{dV(\phi)/d\phi} = \frac{1}{2\sqrt{I}}\left(1 - \cos\left(\frac{2\pi}{T}\phi\right)\right) \tag{15}$$

We can use $\phi \in [0, T[$ and $\theta \in \mathbb{T}$ to see that (15) can be expressed as

$$PRC(\theta) = \frac{1}{2\sqrt{I}}(1 + \cos\theta) \tag{16}$$

which is the magnitude with which I excites the model (8), [18]. Analysis of the *PRC* thus allows us to study how the bifurcation of θ with magnitude I occurs.

The *PRC* is always positive, which indicates that a positive bifurcation will advance the time of the spike, and vice versa.

4.5 Networks of theta neurons

We can easily extend the model to networks of neurons:

$$\dot{\theta}_i = (1 - \cos\theta_i) + (1 + \cos\theta_i) \cdot [\eta_i + \kappa \cdot I_i(t)] \qquad \theta_i \in \mathbb{T}^N \tag{17}$$

$$I_i(t) = \frac{1}{\langle k \rangle} \sum_{j=1}^{N} A_{ij} \cdot \mathcal{P}_n(\theta_j) \tag{18}$$

where the excitability η_i is drawn from a distribution $g(\eta|\eta_0, \sigma)$ and $\mathcal{P}(\theta) = a_n(1 - \cos\theta)^n$ models synaptic coupling by a pulse-shaped signal, emitted when a neuron fires. n models the sharpness of the pulse, and a_n is a normalisation constant. We will take $n = 2$ from here in as in [15], [7], [19]. Another type of coupling is proportional to the difference in voltage between neurons [19]. Note that for a fully connected network, (18) reduces to the scenarios in [15] and [19].
In (17) we see everything come together: changes to the phase θ_i come from $\dot{\theta}_i$, which in turn depends on I, which depends on all phases in the network.

5 Mean Field Reductions

5.1 The Ott-Antonsen manifold for fully connected networks

Lorem ipsum dolor sit amet, consectetur adipiscing elit. Quisque nisl eros, pulvinar facilisis justo mollis, auctor consequat urna. Morbi a bibendum metus. Donec scelerisque sollicitudin enim eu venenatis. Duis tincidunt laoreet ex, in pretium orci vestibulum eget.

5.2 Extension to arbitrary network topologies

Lorem ipsum dolor sit amet, consectetur adipiscing elit. Quisque nisl eros, pulvinar facilisis justo mollis, auctor consequat urna. Morbi a bibendum metus. Donec scelerisque sollicitudin enim eu venenatis. Duis tincidunt laoreet ex, in pretium orci vestibulum eget.

6 *Investigation:* Mean Field Reductions for undirected graphs

6.1 Directed graphs as permutations

Lorem ipsum dolor sit amet, consectetur adipiscing elit. Quisque nisl eros, pulvinar facilisis justo mollis, auctor consequat urna. Morbi a bibendum metus. Donec scelerisque sollicitudin enim eu venenatis. Duis tincidunt laoreet ex, in pretium orci vestibulum eget.

6.2 Building the adjacency matrix

We can find an exact solution for A given the degree vectors in (2). A_{ij} represents a directed graph, but $A_{ij} \neq A_{ji}$ is not a necessary condition. For the elements of A_{ij} we need to find N^2 number of variables. We have the following constraints:

1. The column- and row-sums of A_{ij} must be equal to $\boldsymbol{k}^{\mathbf{in}}$ and $\boldsymbol{k}^{\mathbf{out}}$, see (1). $2N$ constraints.

2. Self-coupling is mandatory: $A_{ii} = \mathbf{1}$. N constraints.

3. The total number of links is constant: $\sum_{i=1}^{N} \boldsymbol{k}_i^{\mathbf{in}} \equiv \sum_{j=1}^{N} \boldsymbol{k}_j^{\mathbf{out}} \equiv \sum_{i,j=1}^{N} A_{ij}$. 1 constraint.

This means that there are $N^2 - (3N + 1)$ variables to find. Once a solution has been found, A_{ij} can be switched with element A_{ic} if $A_{ij} \neq A_{ic}$ and A_{rj} with A_{rc}, which yields a new feasible solution. The number of switches one can make is high, and therefore we can simply try a stochastic approach to obtain A:

1. Choose a random row $i \in [1, N]$. $A_{i,i} = 1$, so we need $m = \boldsymbol{k}_i^{\mathbf{in}} - 1$ elements that are 1.

2. Perform $F(\boldsymbol{k}_j^{\mathbf{out}}, j \neq i)$ and therein find the indices $\boldsymbol{\ell}$ of the m first largest elements.

3. Set $A_{il} = 1 \ \forall \ l \in F^{-1}(\boldsymbol{\ell})$.

Algorithms that find the largest value in a vector start from the first or the last element. The permutation allows us to find different maxima every time by shuffling the vector.

6.3 Results

Lorem ipsum dolor sit amet, consectetur adipiscing elit. Quisque nisl eros, pulvinar facilisis justo mollis, auctor consequat urna. Morbi a bibendum metus. Donec scelerisque sollicitudin enim eu venenatis. Duis tincidunt laoreet ex, in pretium orci vestibulum eget.

7 Hebbian Learning

7.1 Fire and Wire

Lorem ipsum dolor sit amet, consectetur adipiscing elit. Quisque nisl eros, pulvinar facilisis justo mollis, auctor consequat urna. Morbi a bibendum metus. Donec scelerisque sollicitudin enim eu venenatis. Duis tincidunt laoreet ex, in pretium orci vestibulum eget.

7.2 Anti-hebbian learning

Lorem ipsum dolor sit amet, consectetur adipiscing elit. Quisque nisl eros, pulvinar facilisis justo mollis, auctor consequat urna. Morbi a bibendum metus. Donec scelerisque sollicitudin enim eu venenatis. Duis tincidunt laoreet ex, in pretium orci vestibulum eget.

8 Plasticity

8.1 Intrinsic plasticity

Lorem ipsum dolor sit amet, consectetur adipiscing elit. Quisque nisl eros, pulvinar facilisis justo mollis, auctor consequat urna. Morbi a bibendum metus. Donec scelerisque sollicitudin enim eu venenatis. Duis tincidunt laoreet ex, in pretium orci vestibulum eget.

8.2 Spike-timing dependant plasticity

Lorem ipsum dolor sit amet, consectetur adipiscing elit. Quisque nisl eros, pulvinar facilisis justo mollis, auctor consequat urna. Morbi a bibendum metus. Donec scelerisque sollicitudin enim eu venenatis. Duis tincidunt laoreet ex, in pretium orci vestibulum eget.

9   *Investigation:* Emerging Network Topologies

9.1   Redefinition of the network

Lorem ipsum dolor sit amet, consectetur adipiscing elit. Quisque nisl eros, pulvinar facilisis justo mollis, auctor consequat urna. Morbi a bibendum metus. Donec scelerisque sollicitudin enim eu venenatis. Duis tincidunt laoreet ex, in pretium orci vestibulum eget.

9.2   Results

Lorem ipsum dolor sit amet, consectetur adipiscing elit. Quisque nisl eros, pulvinar facilisis justo mollis, auctor consequat urna. Morbi a bibendum metus. Donec scelerisque sollicitudin enim eu venenatis. Duis tincidunt laoreet ex, in pretium orci vestibulum eget.

9.3   Discussion

Lorem ipsum dolor sit amet, consectetur adipiscing elit. Quisque nisl eros, pulvinar facilisis justo mollis, auctor consequat urna. Morbi a bibendum metus. Donec scelerisque sollicitudin enim eu venenatis. Duis tincidunt laoreet ex, in pretium orci vestibulum eget.

10 Conclusion and discussion

Test citations: ln [19]

11 References

[1] *Human Brain Project.*, 2017. https://www.humanbrainproject.eu/en/. Accessed: 28.05.2020.

[2] C. Börgers, *An Introduction to Modeling Neuronal Dynamics.* Texts in Applied Mathematics. Springer International Publishing, 2018.

[3] *The Nobel Prize in Physiology or Medicine 1963.*, 2009. https://www.nobelprize.org/prizes/medicine/1963/speedread/. Accessed: 28.05.2020.

[4] S. Herculano-Houzel, *The Human Brain in Numbers: A Linearly Scaled-up Primate Brain. Frontiers in human neuroscience* **3** (11, 2009) 31.

[5] E. Bullmore and D. Bassett, *Brain Graphs: Graphical Models of the Human Brain Connectome. Annual review of clinical psychology* **7** (04, 2010) 113–40.

[6] E. Ott and T. M. Antonsen, *Low Dimensional Behavior of Large Systems of Globally Coupled Oscillators.* arXiv:0806.0004 [nlin.CD].

[7] S. Chandra, D. Hathcock, K. Crain, T. Antonsen, M. Girvan, and E. Ott, *Modeling the Network Dynamics of Pulse-Coupled Neurons. Chaos (Woodbury, N.Y.)* **27** (03, 2017) 10.

[8] P. Erdos and A. Rényi, *On Random Graphs I. Publicationes Mathematicae* **6** (1959) 290–297.

[9] A. Barabási, *Network Science.* Cambridge University Press, 2016. https://books.google.dk/books?id=iLtGDQAAQBAJ.

[10] A.-L. Barabási and E. Bonabeau, *Scale-Free Networks. Scientific American* **288** no. 60-69, (2003) 50–59. http://www.nd.edu/~networks/PDF/Scale-Free%20Sci%20Amer%20May03.pdf.

[11] C. I. Del Genio, T. Gross, and K. E. Bassler, *All Scale-Free Networks Are Sparse. Phys. Rev. Lett.* **107** (Oct, 2011) 178701. https://link.aps.org/doi/10.1103/PhysRevLett.107.178701.

[12] F. C. Hoppensteadt and E. M. Izhikevich, *Canonical Neural Models.*, 2001.

[13] A. Hodgkin, *The local electric changes associated with repetitive action in a non-medullated axon. The Journal of physiology* **107** no. 2, (March, 1948) 165—181. https://www.ncbi.nlm.nih.gov/pmc/articles/pmid/16991796/?tool=EBI.

[14] B. Ermentrout and N. Kopell, *Parabolic Bursting in an Excitable System Coupled with a Slow Oscillation. Siam Journal on Applied Mathematics - SIAMAM* **46** (04, 1986) 233–253.

[15] T. Luke, E. Barreto, and P. So, *Complete Classification of the Macroscopic Behavior of a Heterogeneous Network of Theta Neurons. Neural Computation* **25** (12, 2013) 1–28.

[16] B. Gutkin, *Theta-Neuron Model.* Springer New York, New York, NY, 2013. https://doi.org/10.1007/978-1-4614-7320-6_153-1.

[17] F. A. Pérez, *Phase-responsiveness transmission in a network of quadratic integrate-and-fire neurons. Universitat Politècnica de Catalunya, Facultat de Matemàtiques i Estadística* (January, 2020) . Bachelor Thesis.

[18] B. Ermentrout, *Type i Membranes, Phase Resetting Curves, and Synchrony* Neural Comput. **8** no. 5, (July, 1996) 979–1001. https://doi.org/10.1162/neco.1996.8.5.979.

[19] C. Bick, M. Goodfellow, C. Laing, and E. Martens, *Understanding the dynamics of biological and neural oscillator networks through exact mean-field reductions: a review.* Journal of Mathematical Neuroscience **10** no. 1, (Dec., 2020) .

A   Appendix

A.1   Transformation to the QIF model

We prove that the transformation (9) holds from the *QIF* model (10) to the Theta model (8).

$$V \equiv \tan\left(\frac{\theta}{2}\right) \quad \longrightarrow \quad \frac{dV}{dt} = \frac{1}{2\cos^2\left(\frac{\theta}{2}\right)}\frac{d\theta}{dt}$$

Insert into $\frac{dV}{dt} = V^2 + I$:

$$\frac{d\theta}{dt} = 2\left(\cos^2\left(\frac{\theta}{2}\right)\cdot\tan^2\left(\frac{\theta}{2}\right) + \cos^2\left(\frac{\theta}{2}\right)\cdot I\right) = 2\left(\sin^2\left(\frac{\theta}{2}\right) + \cos^2\left(\frac{\theta}{2}\right)\cdot I\right)$$

Using $\cos^2\left(\frac{\theta}{2}\right) = \frac{1+\cos\left(\frac{\theta}{2}\right)}{2}$ and $\sin^2\left(\frac{\theta}{2}\right) = \frac{1-\cos\left(\frac{\theta}{2}\right)}{2}$:

$$\dot{\theta} = 2\left(\frac{1-\cos\theta}{2} + \left(\frac{1+\cos\theta}{2}\right)\cdot I\right) = (1-\cos\theta) + (1+\cos\theta)\cdot I$$

This proves that the transformation (9) is correct.

A.2   Solutions to the QIF model

Depending on the value of I, we can distinguish multiple solutions [17]. In all cases we can integrate through the separation of variables. Solutions are bound to start at $V(t_0)$, right after a spike has occured at $t = t_0$.

A.2.1   Solving for $I < 0$

$$\int_{V(t_0)}^{V(t)} \frac{dv}{v^2 - \tilde{I}^2} = \int_{V(t_0)}^{V(t)} \frac{dv}{(v+\tilde{I})(v-\tilde{I})} = \frac{1}{2\tilde{I}}\int_{V(t_0)}^{V(t)} \frac{dv}{v-\tilde{I}} - \frac{1}{2\tilde{I}}\int_{V(t_0)}^{V(t)} \frac{dv}{v+\tilde{I}}$$

$$= \frac{1}{2\tilde{I}}\log\left(1 - \frac{2\tilde{I}}{v+\tilde{I}}\right)\Big|_{V(t_0)}^{V(t)} = \int_{t_0}^{t} d\tau = t - t_0$$

$$V(t) = \lim_{V(t_0)\to-\infty} \frac{2\sqrt{-I}}{1 - \left(1 - \frac{2\sqrt{-I}}{V(t_0)+\sqrt{-I}}\right)\cdot e^{2(t-t_0)\sqrt{-I}}} - \sqrt{-I}$$

$$= \frac{2\sqrt{-I}}{1 - e^{2(t-t_0)\sqrt{-I}}} - \sqrt{-I}$$

A.2.2   Solving for $I = 0$

$$\int_{V(t_0)}^{V(t)} \frac{dv}{v^2} = \frac{1}{v}\Big|_{V(t_0)}^{V(t)} = -\frac{1}{V(t)} + \frac{1}{V(t_0)} = \int_{t_0}^{t} d\tau = t - t_0$$

$$V(t) = \lim_{V(t_0)\to-\infty} \frac{V(t_0)}{1 - V(t_0)(t-t_0)} \overset{\text{H}}{\underset{\infty}{=}} \frac{-1}{t - t_0}$$

A.2.3 Solving for $I > 0$

$$\int_{V(t_0)}^{V(t)} \frac{dv}{v^2 + I} = \int_{V(t_0)}^{V(t)} \frac{I}{\left(\frac{v}{\sqrt{I}}\right)^2 + 1} \, dv \overset{x=\frac{v}{\sqrt{I}}}{\underset{dx=\frac{dv}{\sqrt{I}}}{=}} \int_{\frac{V(t_0)}{\sqrt{I}}}^{\frac{V(t)}{\sqrt{I}}} \frac{I}{x^2 + 1} \, dx = \frac{1}{\sqrt{I}} \arctan(x) \Big|_{\frac{V(t_0)}{\sqrt{I}}}^{\frac{V(t)}{\sqrt{I}}}$$

$$= \frac{1}{\sqrt{I}} \left(\arctan\left(\frac{V(t)}{\sqrt{I}}\right) - \arctan\left(\frac{V(t_0)}{\sqrt{I}}\right) \right) = \int_{t_0}^{t} d\tau = t - t_0$$

$$V(t) = \lim_{V(t_0) \to -\infty} \sqrt{I} \cdot \tan\left((t - t_0)\sqrt{I} + \arctan\left(\frac{V(t_0)}{\sqrt{I}}\right) \right) = \sqrt{I} \cdot \tan\left((t - t_0)\sqrt{I} - \frac{\pi}{2} \right)$$

$$= \sqrt{I} \cdot \cot\left((t - t_0)\sqrt{I} \right)$$

A.3 Frequency response of the neuron models

The integral is solved like before, but now with the conditions of the spike:

$$T = \lim_{a \to \infty} \int_{-a}^{a} \frac{I}{\left(\frac{v}{\sqrt{I}}\right)^2 + 1} \, dv \overset{x=\frac{v}{\sqrt{I}}}{\underset{dx=\frac{dv}{\sqrt{I}}}{=}} \lim_{a \to \infty} \int_{\frac{-a}{\sqrt{I}}}^{\frac{a}{\sqrt{I}}} \frac{I}{x^2 + 1} \, dx = \lim_{a \to \infty} \frac{1}{\sqrt{I}} \arctan(x) \Big|_{\frac{-a}{\sqrt{I}}}^{\frac{a}{\sqrt{I}}}$$

$$= \frac{1}{\sqrt{I}} \left(\frac{\pi}{2} - \left(-\frac{\pi}{2} \right) \right) = \frac{\pi}{\sqrt{I}}$$

So the frequency of oscillation is proportional to $\sqrt{I}$.

A.4 Jacobian of the Ott-Antonsen manifold
A.5 Jacobian of the Ott-Antonsen extended manifold